RESEARCH ARTICLE

WILEY

Neural representations of the amount and the delay time of reward in intertemporal decision making

Qiang Wang[1,2,3] (ID) | Yajie Wang[2] | Pinchun Wang[4] | Maomiao Peng[5] |
Manman Zhang[1,2,3] | Yuxuan Zhu[2] | Shiyu Wei[2] | Chuansheng Chen[6] |
Xiongying Chen[7,8] | Shan Luo[9,10] | Xuejun Bai[1,2,3]

[1]Key Research Base of Humanities and Social Sciences of the Ministry of Education, Academy of Psychology and Behavior, Tianjin Normal University, Tianjin, China

[2]Faculty of Psychology, Tianjin Normal University, Tianjin, China

[3]Tianjin Social Science Laboratory of Students' Mental Development and Learning, Tianjin, China

[4]Faculty of Education, Tianjin Normal University, Tianjin, China

[5]Department of Psychology, University of Arizona, Tucson, Arizona

[6]Department of Psychological Science, University of California, Irvine, California

[7]The National Clinical Research Center for Mental Disorders & Beijing Key Laboratory of Mental Disorders, Beijing Anding Hospital, Capital Medical University, Beijing, China

[8]Advanced Innovation Center for Human Brain Protection, Capital Medical University, Beijing, China

[9]Department of Internal Medicine, Division of Endocrinology, Keck School of Medicine of the University of Southern California, Los Angeles, California

[10]Department of Psychology, University of Southern California, Los Angeles, California

Correspondence
Xuejun Bai, Faculty of Psychology, Tianjin Normal University, Tianjin, 300387, China.
Email: bxuejun@126.com

Shan Luo, Department of Internal Medicine, Division of Endocrinology, Keck School of Medicine of the University of Southern California, Los Angeles, CA 90033.
Email: shanluo@usc.edu

Abstract

Numerous studies have examined the neural substrates of intertemporal decision-making, but few have systematically investigated separate neural representations of the two attributes of future rewards (i.e., the amount of the reward and the delay time). More importantly, no study has used the novel analytical method of representational connectivity analysis (RCA) to map the two dimensions' functional brain networks at the level of multivariate neural representations. This study independently manipulated the amount and delay time of rewards during an intertemporal decision task. Both univariate and multivariate pattern analyses showed that brain activity in the dorsomedial prefrontal cortex (DMPFC) and lateral frontal pole cortex (LFPC) was modulated by the amount of rewards, whereas brain activity in the DMPFC and dorsolateral prefrontal cortex (DLPFC) was modulated by the length of delay. Moreover, representational similarity analysis (RSA) revealed that even for the regions of the DMPFC that overlapped between the two dimensions, they manifested distinct neural activity patterns. In terms of individual differences, those with large delay discounting rates (k) showed greater DMPFC and LFPC activity as the amount of rewards increased but showed lower DMPFC and DLPFC activity as the delay time increased. Lastly, RCA suggested that the topological metrics (i.e., global and local

efficiency) of the functional connectome subserving the delay time dimension inversely predicted individual discounting rate. These findings provide novel insights into neural representations of the two attributes in intertemporal decisions, and offer a new approach to construct task-based functional brain networks whose topological properties are related to impulsivity.

1 | INTRODUCTION

Intertemporal decision-making is ubiquitous in daily life and has been considered a crucial factor in individuals' development and success. In general, people are more likely to choose immediate-but-smaller rewards than delayed-but-larger rewards. This common phenomenon is known as temporal discounting, namely, the subjective value of future benefits devalues as the time to delivery increases (Ainslie, 1975; Samuelson, 1937). Steepness of the discounting rates has been associated with real world problems such as substance abuse (Bickel, Odum, & Madden, 1999), pathological gambling (Alessi & Petry, 2003), and attention deficit hyperactivity disorder (ADHD) (Paloyelis, Asherson, Mehta, Faraone, & Kuntsi, 2010).

Previous functional imaging studies have indicated that decision-makers with higher discounting rates (k) frequently exhibit hyper-activation in the valuation network (McClure, Laibson, Loewenstein, & Cohen, 2004) and hypoactivation in the prospection (Peters & Büchel, 2011) and cognitive control networks (Figner et al., 2010). Because the subjective value of future rewards and k are dependent on two attributes of the rewards: the amount and the length of delay (Kable & Glimcher, 2007; Rangel, Camerer, & Montague, 2008), researchers have also been interested in understanding how the brain represents these two attributes. Earlier studies implicated the brain areas of the ventromedial prefrontal cortex (VMPFC), ventral striatum (VS), and posterior cingulate cortex (PCC) in the processing of the amount of rewards, and the brain regions of the dorsolateral prefrontal cortex (DLPFC) and posterior parietal cortex (PPC) in the processing of the delay time (Ballard & Knutson, 2009; Li et al., 2013). Subsequent research showed that the dorsomedial prefrontal cortex (DMPFC) was also associated with the processing of delay time. Specifically, an fMRI study showed that blood-oxygen-level-dependent (BOLD) signal change in the DMPFC was sensitive to delay time (Massar, Libedinsky, Chee, Huettel, & Chee, 2015). A morphological analysis also revealed that DMPFC atrophy was linked to attenuated sensitivity to delay time among patients with Alzheimer's disease and healthy control subjects (Beagle et al., 2020).

The above-mentioned studies, however, all utilized traditional univariate (voxel-wise) activation analysis. Such analytical approach has been found to be less sensitive to distributed coding of information than the newer method of multivoxel pattern analysis (MVPA) (Jimura & Poldrack, 2012; Kahnt, 2018; Zha et al., 2019). In contrast, MVPA concerns the spatial distributed patterns of voxel activity that can be used to decode the specific cognitive processes (Ritchie, Kaplan, & Klein, 2019). Using MVPA, our previous study (Wang et al., 2014) manipulated the amount of future rewards (with fixed length of delay, 120 days) and found distributed neural representation of the amount of future rewards in the DMPFC. Here, we extended from prior studies to manipulate both the amount and the delay time of rewards simultaneously and independently, in order to examine distributed neural representations of these two attributes.

In addition to using multivariate analyses, the current study also used a novel network construction approach (i.e., representational connectivity analysis [RCA]) to examine the functional networks involved in the processing of the two attributes during intertemporal decision-making (Zhao et al., 2017). This approach measures the degrees of similarity of the representational spaces of different regions through a "second-order representational similarity analysis (RSA)" (Kriegeskorte, Mur, & Bandettini, 2008). Traditional connectivity analyses (both functional and structural) have revealed significant associations between small-world properties of human brain and intertemporal decision-making. Specifically, individual differences in discounting rates were found to be related to global topological organization including small-world and rich-club regimes in both functional and structural connectivity networks (Chen, Hu, Chen, & Feng, 2019; Wang, Lv, He, & Xue, 2020a) and the network-based (Li et al., 2013) and voxel-based (Cai, Chen, Liu, Zhu, & Yu, 2020; Wang et al., 2020b) intrinsic functional connectivity during resting-state functional magnetic resonance imaging (fMRI). Such individual differences are recently investigated via connectome-based prediction model (CPM), which is widely applied to explore the brain connectivity-behavior associations due to reliable, simple, and highly efficient characteristics (Shen et al., 2017). However, it remains unknown about amount-related and delay-related function-specific representational brain networks, and their associations with discounting rate. Relative to RCA, traditional connectivity analysis might only provide relatively little information related to specific amount and delay representations, which is thought to play a critical role in understanding cognitive and neural mechanisms of decision-making based on recent attribute-wise decision theory. Thus, we used RCA approach to reconstruct function-specific brain networks corresponding to amount and delay time, and used graph theoretical analysis to establish the link between

topological metrics of the brain networks related to the two attributes and temporal discounting rates.

2 | MATERIALS AND METHODS

2.1 | Subjects

Twenty-four subjects (8 males; age, 21.21 ± 1.22 years old) participated in the study. Five volunteers were excluded from final analyses due to one of the following two reasons: large head motion [3 subjects; mean framewise displacement (FD) > 0.5 mm in any one of three runs], or misunderstanding of task instructions (2 subjects). All subjects were free from neurological or psychiatric disorders. Informed written consent was obtained from subjects before the experiment. This study was approved by the Institutional Review Board of the Faculty of Psychology at Tianjin Normal University in China.

2.2 | Intertemporal choice task

Figure 1 depicts the stimuli and the experimental procedures of the intertemporal choice task. Such experimental procedure has also been applied in another study that provided more detailed information (Wang et al., 2021). Subjects were instructed to choose between a fixed immediate reward (always RMB 40, which is about US$6) and a delayed reward that varied across trials. To independently estimate the neural responses to the amount and delay of future rewards, the

two dimensions were manipulated independently and orthogonally, with the amount ranging from RMB 40 to 115 (16 levels in RMB 5 increments), and the delay varying from 1 to 150 days (16 levels in 9-day or 10-day increments). These ranges were chosen based on our previous study (Wang et al., 2014) and an additional pilot study of an independent sample (n = 12). All the possible combinations of each amount and delay level yielded a total of 256 trials. These trials were divided pseudo-randomly into three runs (e.g., run1 = 86 trials, run2 = 85 trials, and run3 = 85 trials), with each run having the same number of amount/delay time levels (e.g., 16 levels of amount and delay time with 5–6 trials, respectively). We utilized an event-related fMRI design and optimized the timing and order of stimulus presentation using optseq2 in order to maximize the estimation efficiency (Dale, 1999).

Following a similar procedure done in a previous study (Kable & Glimcher, 2007), for each trial, the amount and delay time of the future reward were shown on the screen but the fixed but immediate reward was told to the participant beforehand and was not shown. The amount and the delay time appeared side by side divided by a vertical line (see Figure 1) and whether the amount or the delay time appeared on the right side was determined randomly. Subjects were asked to respond as quickly as possible within 3-s trial duration. If no response was made within this window, the task continued to the next trial. The trials with no responses (ranging from 0 to 7 trials, mean ± SD = 1.52 ± 1.84 trials) were modeled as a separate regressor of no interest in the general linear model (GLM). To encourage subjects to reflect true preference for each decision rather than a fixed decision rule (Tom, Fox, Trepel, & Poldrack, 2007), we required them to indicate one of four responses to each decision (strongly choose
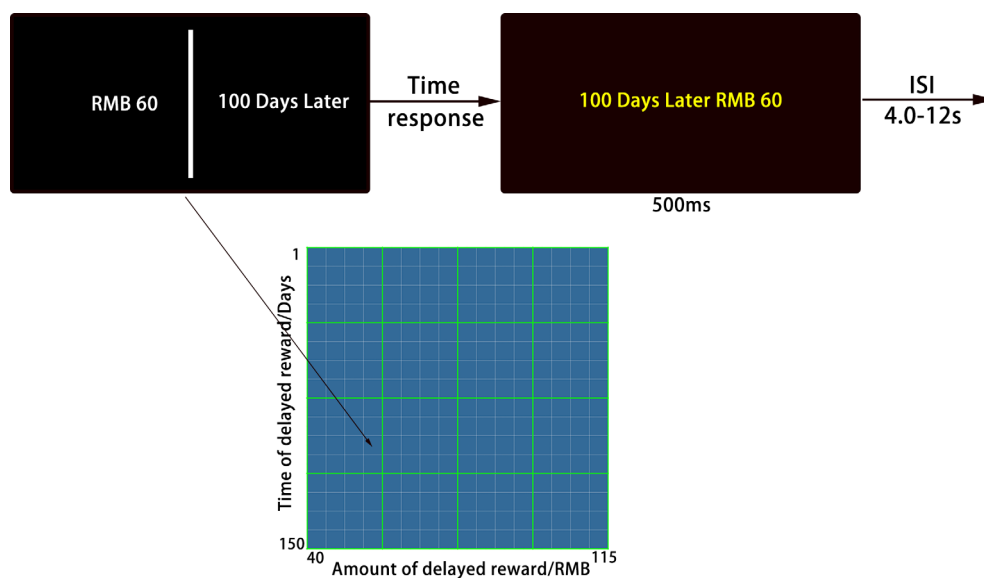

FIGURE 1 An illustration of the event-related experimental design. During each trial, the amount and delay time of a future reward were presented side by side divided by a vertical line on the screen (for 3 s), but the fixed immediate option (RMB 40) was told to the participants beforehand and was not displayed visually. Participants were required to make a decision between the immediate and delayed alternatives based on their preference. The chosen option turned to yellow after choice. The amount and time of delayed rewards for each trial were sampled from the amount/time matrix, shown here as one sample trial. A decision from each cell in this 16 × 16 matrix was presented during scanning, but the data were collapsed into a 4 × 4 matrix for analysis. The interstimulus interval (ISI) was jittered to optimize design efficiency

the immediate option, weakly choose the immediate option, weakly choose the delayed option, and strongly choose the delayed option) using a four-button response box. After each decision, the chosen option turned yellow as the feedback.

At the end of the experiment, all participants received the non-contingent compensation of RMB 50 plus a bonus based on the amount they earned on one randomly chosen trial (i.e., the participants did not receive the actual total amount earned). In other words, each participant received 50+ either 40 (for choosing the immediate reward, with the total amount paid at the end of the experiment) or 45–115 (for choosing the delayed reward, with noncontigent compensation paid at the end of the experiment and the bonus paid as indicated by the delay time) in RMB.

2.3 | Functional imaging procedure

Imaging data were collected using a Siemens Prisma 3 T scanner with a 64-channel head coil at the Center for MRI Research of Tianjin Normal University. Subjects laid supine on the scanner bed and viewed visual stimuli back-projected onto a screen through a mirror attached to the head coil. Foam pads were used to minimize head motion. The experiment was programmed and run with MATLAB (MathWorks) and Psychtoolbox with version of 3.1 (www.psychtoolbox.org) on a PC laptop. Subjects' responses were collected using an MRI-compatible button box.

For each functional session, T2*-weighted functional images were acquired with a simultaneous multi-slice (SMS) sequence supplied by Siemens. The following parameters were used: repetition time (TR) = 2,000 ms; echo time (TE) = 30 ms; GRAPPA factor = 2; multi-band acceleration factor = 2; flip angle = 90°; field-of-view (FOV) = 224×224 mm^2; slice thickness = 2 mm; slice gap = 0.3 mm; voxel size = $2 \times 2 \times 2$ mm^3. The scan time of each run was 8 min 4 s, and thus 242 volumes were acquired for each run. The slices were tilted approximately 30° clockwise from the AC–PC plane to obtain better signals in the orbitofrontal cortex. Additionally, MP-RAGE T1-weighted image for each subject was also obtained (192 slices, TR = 2,530 ms, TE = 2.98 ms, multiband factor = 2, flip angle = 7°, FOV = 224×256 mm^2; voxel size = $0.5 \times 0.5 \times 1$ mm^3).

2.4 | Behavioral data analysis

Statistical analyses of the behavioral data were performed using MATLAB (MathWorks). Subjects' indifference points were firstly calculated at each delay to fit individualized discounting curves. After collapsing strong/weak responses into immediate (0) and delay (1) categories, subjects' choices for a given delay were extracted, and then fitted to a logistic function to determine the amount at which there was a 50% probability of choosing the immediate versus the delayed option (i.e., the indifference point). Subjective discounted value (SDV) of the delayed option relative to the immediate option (RMB 40) was calculated for each delay (SDV = 40/indifference point). Previous

studies (Ballard & Knutson, 2009; Green & Myerson, 1996) have demonstrated that the hyperbolic discounting model fits individuals' behavior equally well as other models, and has been widely adopted in both human and animal studies (Green & Myerson, 2004). Therefore, we calculated individuals' discounting rate by using the hyperbolic discounting function (SDV = $1/[1 + k \times D]$), where D is the length of the delay in days and k is an individual discounting parameter. Larger k value indicates greater impulsivity, whereas smaller k value indicates more patience. For cross-validation and comparison, we also fit each subject's discount curve with a sum of double exponential functions: SDV = $0.5 \times (e^{-\beta D} + e^{-\delta D})$, where β and δ are subject-specific constants. The double exponential model is one formulation of an economic model that explains hyperbolic-like discounting by the two systems. One is the β system that discounts more steeply while the other is δ system that discounts less steeply. Not surprisingly, as the function can account for hyperbolic-like discounting, the double exponential function (average accuracy of prediction = 89.42 ± 4.26%) fit the data marginally better than single parameter hyperbolic function (average accuracy of prediction = 88.46 ± 4.42%) ($t_{[18]}$ = 2.095, p = .051). Table S1 provides more details.

2.5 | fMRI data analysis

Image preprocessing and statistical analyses were performed by using the FMRI Expert Analysis Tool (version 6.00; part of the FSL package; http://www.fmrib.ox.ac.uk/fsl). The first four volumes before the task were automatically discarded by the scanner to allow for T1 equilibrium. The remaining images were then realigned to correct for head movements. Data were spatially smoothed by using a 5-mm full width at half maximum Gaussian kernel and filtered in the temporal domain using a nonlinear high-pass filter with a 90 s cutoff. EPI images were first registered to the MPRAGE structural images and then into MNI standard space, using affine transformations (Jenkinson & Smith, 2001). Registration from MPRAGE structural images to standard space was further refined using FNIRT nonlinear registration. Statistical analyses were performed in the native image space, with the statistical maps normalized to the standard space, before higher-level analysis.

Firstly, traditional parametric fMRI design was used to identify the neural correlates of the amount and delay of future rewards. The data were modeled at the first level using a GLM within FSL's FILM module. Four parametric regressors were included during the decision-making period starting from the presentation of inter-temporal alternatives and ending when subjects responded: (a) the overall task regressor (1 for each trial); (b) the amount of future reward; (c) the delay of future reward; and (d) reaction time (RT; Sripada, Gonzalez, Phan, & Liberzon, 2011). For all the models, each regressor (except for the task regressor) was first demeaned and normalized to the same range (−1 vs. 1) and then convolved with the double-gamma canonical hemodynamic response function. Trials with no valid response were modeled as a separate regressor of no interest.

Previous studies have suggested that vmPFC, nucleus accumbens (NAcc), and posterior cingulate cortex (PCC) might represent different

value signals, such as the relative value (Wang et al., 2014), the subjective value (Kable & Glimcher, 2007), the chosen value (Kable & Glimcher, 2009), the summed value (Sripada et al., 2011), and even the amount of delayed reward (Ballard & Knutson, 2009; Li et al., 2013). These values were calculated as follow: relative value = abs (40– subjective value), summed value = (40+ subjective value). The chosen value was calculated as the subjective value of the option subjects chosen (i.e., if immediate option chosen, the chosen value is 40; Otherwise, the chosen value is the subjective value of delayed reward). These ROIs were further defined as the peak point with a radius of 9 mm based on the article of Kable and Glimcher (2007) (VMPFC, Talairach coordinate = −3, 38, 13; NAcc = −12, 5, 1; PCC = −3, −43, 37). Here, we applied several simple GLM models with only the task and one of these value regressors mentioned above to examine whether these regions encoded the different value signals or the amount of future reward in the experiment. Given the collinearity of the subjective value, chosen value, summed value, and relative value, we expected to see consistent neural responses across these value regressors in these regions.

A second-level analysis was performed using a fixed-effect model where all three functional runs were combined within individual participants. Finally, these second-level results were then fed into a random-effect model for group analysis and regression analysis for each individual's discounting rate using a FLAME1 model. Considering the impacts of head motion on the functional activations, the FD was additionally included as a confounding factor in the main GLM. Group images were thresholded using cluster detection statistics, with a height threshold of $z > 3.1$ and a cluster probability of $p < .05$, corrected for whole-brain multiple comparisons using Gaussian Random Field Theory.

To evaluate signal change for each level of amount and delay of future rewards, we constructed two additional models to estimate the brain signal change for each of the 16 levels of amount and delay of future rewards, respectively. For each model, all trials with the same amount (or delay) information were grouped into separate regressors (16 in total); the delay time (or amount) and the RT were included as covariates of no interest. In one version of the model, we used the smoothed data and fitted the value function. In another version, we used the unsmoothed data to conduct the MVPA and network construction via RCA.

By using a fast event-related design, we were able to present all possible pairs of amount and delay levels at a relatively wide range and small steps, which improves the resolution and accuracy of reward representations. A similar method has been employed to examine the neural representations of gain and loss in risky decision-making (Jimura & Poldrack, 2012), and neural representation of immediate and delayed reward in intertemporal choices (Wang et al., 2014).

2.6 | Support vector regression analysis

High-dimensional regression MVPA was performed using a searchlight procedure with a 3-voxel radius. Epsilon-insensitive support vector regression (SVR) (Drucker, Burges, Kaufman, Smola, & Vapnik, 1997) with a linear kernel, as implemented in PyMVPA (http://www.pymvpa.org) (Hanke et al., 2009), was used to estimate the target amount and delay time of future rewards (Jimura & Poldrack, 2012; Wang et al., 2014). Three-fold cross-run validation was used within subjects. For each level of the amount or delay time, test and training data were normalized (i.e., with the mean subtracted out and then divided by SD) across voxels within each region of interest (ROI, including 27 voxels) (i.e., searchlight) (Misaki, Kim, Bandettini, & Kriegeskorte, 2010). This procedure allows the evaluation of the pattern of activity across voxels without contamination from the mean signal differences within the searchlight. Based on previous studies (Jimura & Poldrack, 2012; Wang et al., 2014), the SVR cost parameter was set to 0.001 and the ε parameter was set to 0.01.

Voxel-wise accuracy of SVR prediction was then calculated, defined as the z-transformed Pearson's correlation coefficient between actual and predicted values of the amount or delay of future reward for the left-out BOLD periods. Then, individuals' prediction maps were further smoothed with an isotropic 6 mm FWHM Gaussian kernel. Group analysis used mixed FLAME 1 models to facilitate the comparison with the univariate analyses. Group images were thresholded using cluster detection statistics, with a height threshold of $z > 3.1$ and a cluster probability of $p < .05$, corrected for whole-brain multiple comparisons using Gaussian Random Field Theory.

2.7 | ROI analyses

The clusters showing significant modulation of the amount (DMPFC, LFPC) and delay of reward (DMPFC, DLPFC) were firstly defined as the ROIs. ROIs analyses were conducted by extracting parameter estimates (betas) of each event type from the fitted model and averaging across all voxels in each significant cluster for each subject. Percentage signal changes were computed via the following formula: [contrast image/(mean of run)] × ppheight × 100%, where ppheight is the peak height of the hemodynamic response versus the baseline level of activity (Mumford, 2007).

2.8 | Representational similarity analysis between amount and delay time conditions in DMPFC

The DMPFC ROI was functionally defined with a conjunction analysis of the amount and delay time conditions (i.e., Figures 3a and 4a. Voxel size = 409) (Friston, Penny, & Glaser, 2005). We extracted the signal for each individual voxel within this ROI and investigated the degree of similarity in the fMRI activity patterns between the amount and delay time conditions, using the Pearson correlation coefficient as the similarity metric. Due to unknown the distributions of the representational patterns responsible to the amount and delay time, Spearman's correlational analysis was also utilized to further confirm the robustness of our findings.

2.9 | Functional brain network construction via representational connectivity analysis

In the graph-theoretical analysis, defining the nodes of the brain network is an extremely important step that directly determines the success of brain network construction. Based on numerous previous studies, we utilized both the low-resolution automated anatomical labeling (AAL-90) atlas and high-resolution Power-264 atlas to parcellate the whole brain into different nodes. In addition, calculating the edge of any pair of all nodes is another important step in network construction. In our study, for a given node from AAL-90 or Power-264 atlas, the multivoxel response pattern (beta estimates) for each of the 16 levels of amount or delay time was firstly extracted for each participant separately. Then all possible pairs of these 16 activation patterns (120 in total) were subjected to Pearson correlation analysis, generating a 16×16 matrix of the neural similarity in each node. In order to control for global or similar confounding processing, the mean global signal across the 16-level amount or delay time conditions was subtracted from such analysis initially. Following Kriegeskorte et al. (2008), we calculated representational connectivity among the 90 nodes from low-resolution atlas or among the 264 nodes from high-resolution atlas, using Spearman correlation between the neural similarity patterns of every pair of these nodes, which yielded a 90×90 or 264×264 functional brain network for each amount and delay time condition for each subject.

Next, we quantified the topological metrics of function-specific connectivity networks by the Graph Theoretical Network Analysis (GRETNA) Toolbox (https://www.nitrc.org/project/gretna; Wang et al., 2015). According to previous studies (Rubinov et al., 2009; Rudie et al., 2013), the sparsity-band was chosen from 5 to 40% with step-to-step width of 1% increase as a threshold to determine whether an edge exists between nodes in the amount-related and delay-time-related functional networks. Then, we computed a series of small-world characteristics in both amount and delay-time-related brain networks, including clustering coefficient, shortest path length, Lambda, Gamma, Sigma, and efficiency. The specific algorithm of topological metrics of functional brain network is available from previous literature (Bullmore & Bassett, 2011). Subsequently, the Pearson correlational analysis was used to examine the association between these metrics and delay-discounting rate.

2.10 | Connectome-based prediction modeling

Connectome-based prediction modeling (CPM) has been demonstrated as a reliable and highly efficient approach to identify brain networks associated with a behavioral variable of interest from whole-brain functional connectivity, which can be used to predict behavioral performance at the single subject level (Shen et al., 2017). Here, we employed this method to predict delay-discounting rate (k) using the amount-related and delay-time-related networks constructed by the RCA. In particular, the whole subjects were divided into a training subjects and a testing subject. In the training subjects, each edge in the connectivity matrices was correlated with k using Pearson's correlation analysis with

a statistical significance threshold of $p < .001$ to identify positive and negative predictive networks. Next, we computed single-subject summary value by summing the significant edge weights in positive and negative networks. Then, a predictive model was generated that assumed a linear relationship between the single-subject summary value of connectivity data (independent variable) and the behavioral variable (dependent variable). In the testing subject, the summary value was computed for this subject and was then inputted into the predictive model. The resulting value was the predicted behavioral variable for the current test subject. We employed a leave-one-out cross-validation strategy to test the prediction performance. Finally, model performance was assessed by the magnitude and statistical significance of the Pearson's correlation between actual and predicted k. The statistical significance of the correlation between actual and predicted k was assessed using 10,000 times permutation testing. Based on the null distribution, the p value for the leave-one-out prediction was calculated as the proportion of sampled permutations that were greater than or equal to the true prediction correlation. Due to the potential impacts of head motion on functional connectivity and skewed distribution of k, above-mentioned analyses were conducted again via the log-transformation strategy and including the FD as the covariates.

3 | RESULTS

3.1 | Behavioral results

Individual participants' temporal discounting rates (k) ranged from 0.0019 to 0.0609, similar as those reported in previous studies (Ballard & Knutson, 2009; Kable & Glimcher, 2009). The mean framewise displacement (FD) was 0.161 ± 0.062 and its range was from 0.084 to 0.278. Table S2 provided details on absolute and relative FD for each subject. Discounting rates did not vary significantly as a function of age ($r = 0.269$, $p = .265$), head motion ($r = -0.349$, $p = .144$), or gender ($t_{[18]} = -1.262$, $p = .224$).

Figure 2 shows the average response time and probability of choosing delayed rewards in whole sample. As expected, the probability of
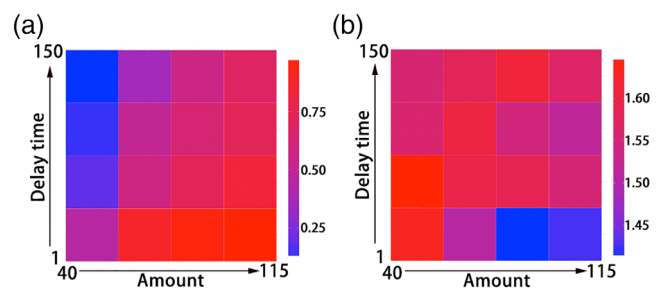

FIGURE 2 Color-coded heatmaps of the average probability of choosing delayed rewards (a) and response time (b) at each level of amount/time combination in whole sample. Red represents higher willingness to choose the delayed rewards (a) and slower response time (B). Blue indicates lower willingness to choose delayed rewards (a) and faster response time (b)

choosing delayed rewards increased with the amount of delayed rewards but decreased with the delay time (Figure 2a). Subjects responded faster when the relative difference between the two options increased (Figure 2b). In terms of the hyperbolic model, the mean modeled accuracy of prediction was 88.46% ($SD = 4.42\%$). One-sample t-test analysis showed significant prediction accuracy than chance ($t_{[18]} = 37.97$, $p < .001$). Table S1 provides more details for each subject.

3.2 | Imaging results

3.2.1 | Brain regions representing the amount of future rewards

Neural representations of the amount and delay of future rewards were examined using both univariate and MVPA. Univariate analysis revealed that the activities in the left DMPFC ($x = -2$, $y = 10$, $z = 52$ in MNI coordinates, peak $Z = 4.48$; Figure 3a) and the left lateral frontal pole cortex (LFPC; xyz: -32, 44, 14, peak $Z = 4.51$; Figure 3c) were negatively correlated with the amount of future rewards. Other brain regions showing similar negative correlations included the right precentral gyrus, left middle temporal gyrus (MTG), bilateral inferior frontal gyrus (IFG), left caudate, left insula, and right thalamus (Figure S1a and Table 1). Focusing on the DMPFC and LFPC, ROIs analysis confirmed the linear decreases in BOLD response as the amount of delayed rewards increased (Figure 3b,d). No brain activations were found to be positively associated with the amount of future rewards.

We then examined whether individual differences in neural responses to the amount of future rewards correlated with individual differences in rates of temporal discounting (k) in the whole-brain analysis. Such brain regions were found in the left DMPFC (xyz: -12, 16, 64, $Z = 4.91$) (Figure 3e) and left LFPC (xyz: -40, 44, -12, $Z = 4.02$) (Figure 3g), whose activations were positively correlated with discounting rates. Similar patterns were also found in the bilateral middle frontal gyrus (MFG), right dorsolateral prefrontal cortex (DLPFC), left insula, right supramarginal gyrus (SMG), and right frontal operculum cortex (Figure S1c and Table 3). Focusing on the DMPFC
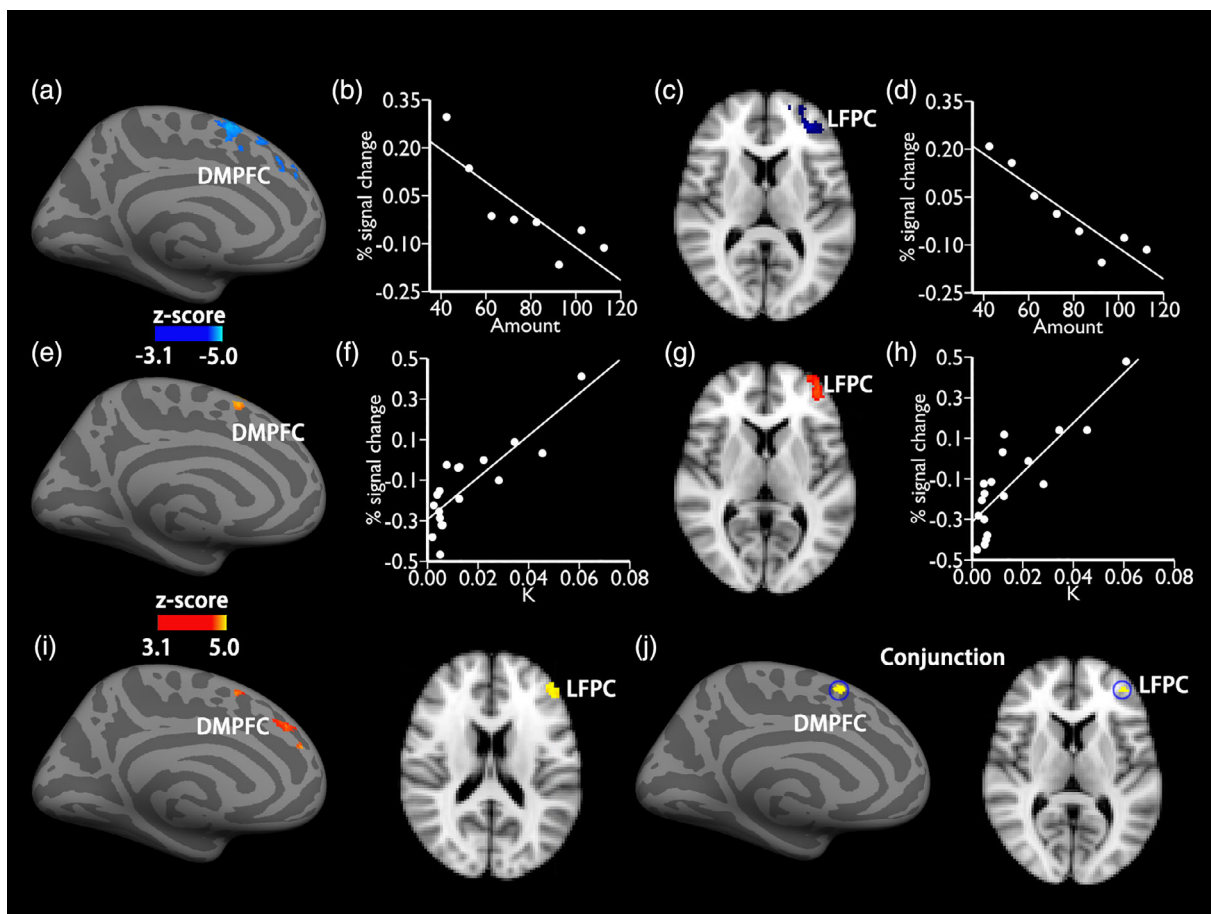

FIGURE 3 The brain regions modulated by the amount of future rewards. The DMPFC (a) and the LFPC (c) showed sensitivity to the amount of future rewards based on the univariate analysis. Percentage signal change was linearly associated with the amount of future rewards in the DMPFC (B) and LFPC (d). Neural responses to the amount of future rewards in the DMPFC (e) and LFPC (G) were positively correlated with discounting rates (k). Percentage signal change was also linearly associated with k in the DMPFC (f) and LFPC (h). The DMPFC and LFPC showed sensitivity to the amount of future rewards in the multivariate analysis (i). Conjunction analysis revealed overlapping regions in the DMPFC and LFPC across these three types (f). The 16-level amount was further collapsed into 8-level in order to reducing noise

TABLE 1 Brain regions represented amount and delay time attributes in univariate analysis

Effect	Brain region	Cluster size (voxels)	MNI coordinates			
			x	y	z	Z
Amount	L DMPFC	975	−2	10	52	4.48
	L LFPC	486	−32	44	14	4.51
	R precentral gyrus	10,455	32	−22	70	5.95
	L middle temporal gyrus	3,296	−56	−38	−2	5.14
	L inferior frontal gyrus	3,238	−58	16	10	5.18
	R inferior temporal gyrus	299	56	−26	−18	4.46
	R thalamus	268	14	−22	6	5.28
	R inferior frontal gyrus	99	58	16	−2	4.34
	L caudate	77	−10	4	18	3.84
	L insular	66	−32	24	4	3.77
Delay time	L DMPFC	2,387	−2	24	58	6.03
	R DLPFC	1,230	52	16	26	4.90
	L lateral occipital cortex	21,911	−42	−72	40	6.65
	R lateral occipital cortex	767	42	−66	44	5.28
	L PCC	1,578	−2	−40	38	5.51
	R occipital fusiform gyrus	1,129	6	−82	−24	5.57
	R inferior temporal gyrus	873	58	−28	−16	5.94
	L caudate	623	−10	12	8	5.11
	L frontal pole	218	−20	44	−18	4.68
	L insular	169	−34	−16	−2	3.90

and LFPC, ROIs analysis confirmed the linear increases in the neural activations in these two brain regions to the increasing amount of delayed rewards (Figure 3f,h). Due to the skewed distribution of k, log-transformed (log k) were used and similar linear correlations were also observed in the DMPFC (r = 0.798, p < .001) and LFPC (r = 0.779, p = .0001) regions. These findings suggested few impacts of the skewed distribution exhibits on the main results. In addition, individual differences in neural responses to the amount of future rewards were not observed negatively correlated with the individual's variation in the discounting rate (k).

In addition, MVPA results revealed that activities in the right DMPFC (xyz: 8, 38, 38, Z = 4.16) and the right LFPC (xyz: −18, 48, 26, Z = 4.23) successfully predicted the amount of future rewards (Figure 3i). Other regions included the left precentral gyrus, bilateral SMG, left inferior temporal gyrus (ITG), left angular gyrus, left superior parietal lobule (SPL), left lateral occipital cortex (LOC), and left MFG (Table 2). Conjunction analysis revealed overlapping brain regions in the DMPFC and LFPC among these three types (Figure 3j), suggesting that DMPFC and LFPC represented the amount of future rewards.

3.2.2 | Brain regions representing the delay time of future rewards

Next, we sought to identify brain regions whose activities were correlated with the delay time of future rewards. Univariate analysis revealed that the activities in the left DMPFC (xyz: −2, 24, 58, Z = 6.03) (Figure 4a) and right DLPFC (xyz: 52, 16, 26, Z = 4.90; Figure 4c) were negatively correlated with the delay time. Other brain regions showing a similar pattern included the right ITG, bilateral LOC, left posterior cingulate cortex (PCC), right occipital fusiform gyrus, left caudate, left frontal pole, and left insular (Figure S1b and Table 1). Focusing on the DMPFC and DLPFC, ROIs analysis confirmed the linear decreases in BOLD response as the delay time increased (Figure 4b,d). However, we did not observed any positive correlations between brain activations and the delay time of future rewards.

We further examined whether individual neural responsiveness to the delay time correlated with the delay discounting rate in the whole-brain analysis. Regression analysis revealed several brain regions, including the right DMPFC (xyz: 10, 16, 68, Z = 5.39) (Figure 4e) and right DLPFC (xyz: 56, 20, 8, Z = 4.64) (Figure 4g), whose activations were negatively correlated with discounting rates. Other brain regions exhibiting similar negative correlations included the right ITG, left postcentral gyrus, right SPL, left LOC, right frontal pole, left PCC, right LOFC, right putamen, and right cerebellum (Figure S1d and Table 3). ROIs analysis further confirmed the linear decreases in the neural activity in these two brain regions as delay time increases (Figure 4f,h). Due to the skewed distribution of k, log-transformed were used and similar linear correlations were also observed in the DMPFC (r = −0.801, p < .001) and DLPFC (r = −0.768, p = .0001) regions. These findings further indicated few impacts of such confounding factors on the main results.

| Effect	Brain region	Cluster size (voxels)	MNI coordinates			
			x	y	z	Z
Amount	R DMPFC	102	8	38	38	4.16
	L LFPC	28	−18	48	26	4.23
	L precentral cortex	406	−30	−14	68	4.68
	R supramarginal gyrus	253	62	−44	36	4.54
	L interior temporal gyrus	160	−62	−36	−20	4.27
	L supramarginal gyrus	154	−56	−52	40	5.07
	L lateral occipital cortex	132	−26	−66	38	4.75
	L angular gyrus	124	−60	−50	16	4.60
	L superior parietal lobule	114	−34	−52	44	5.17
	L middle frontal gyrus	72	−40	6	62	4.35
Delay time	DMPFC	66	0	24	44	3.66
	L DLPFC	159	−44	32	30	4.00
	L central opercular cortex	285	−44	−18	20	4.03
	R precentral cortex	277	44	−16	56	3.46
	L precentral cortex	258	−30	−28	46	4.33
	L superior parietal lobule	77	−46	−42	56	3.92
	L posterior cingulate cortex	70	−4	−26	36	3.40
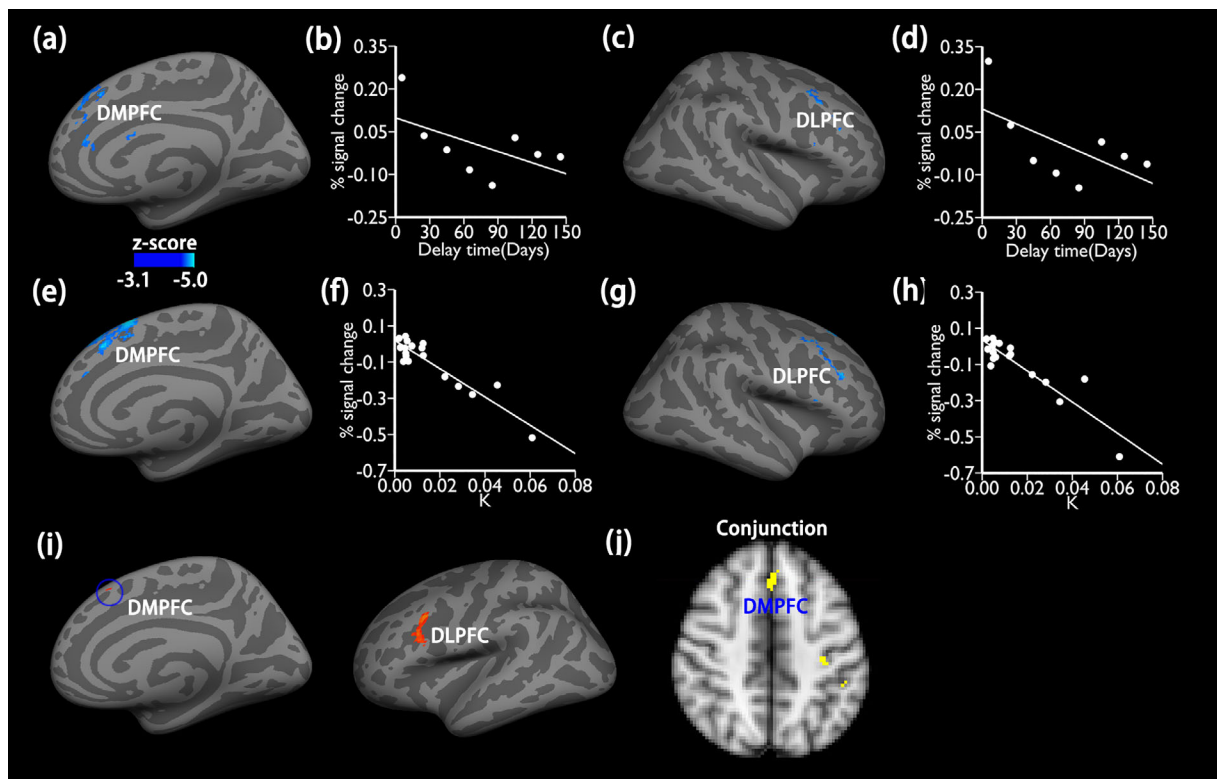
FIGURE 4 The brain regions modulated by the delay length of future rewards. The DMPFC (a) and the DLPFC (c) showed sensitivity to the delay time of future rewards based on the univariate analysis. Percentage signal change was linearly associated with the length of delay time of future reward in the DMPFC (b) and DLPFC (d). Neural responses to the delay time of future rewards in the DMPFC (e) and DLPFC (G) were negatively correlated with discounting rates (k) in the univariate analysis. Percentage signal change was also associated with k in the DMPFC (f) and DLPFC (h). The DMPFC and DLPFC also showed sensitivity to the amount of future rewards in the multivariate analysis (i). Conjunction analysis revealed overlapping regions in the DMPFC across these three types (f). The 16-level delay time was further collapsed into 8-level in order to reducing noise

TABLE 3 Correlations between discounting rate (k) and amount and delay time-related brain regions

Effect	Brain region	Cluster size (voxels)	MNI coordinates			Z
			x	y	z	
Amount versus k	L DMPFC	588	−12	16	64	4.91
	L LFPC	206	−40	44	−12	4.02
	L middle frontal gyrus	389	−48	22	36	4.44
	L insula	308	−40	14	−4	4.21
	R middle frontal gyrus	242	46	30	28	4.46
	R DLPFC	208	36	18	56	4.28
	R supramarginal gyrus	74	46	−40	50	4.23
	R frontal operculum cortex	74	36	26	2	4.18
Delay time versus k	R DMPFC	2,474	10	16	68	5.39
	R DLPFC	70	56	20	8	4.64
	R frontal pole	169	42	52	−2	5.60
	R superior parietal lobule	853	32	−50	48	5.39
	L postcentral gyrus	805	−50	−32	56	4.83
	L lateral occipital cortex	481	−38	−70	48	5.61
	R interior temporal gyrus	257	58	−28	−16	5.24
	L posterior cingulate cortex	162	−2	−32	28	4.70
	R lateral OFC	148	36	28	−4	4.50
	R putamen	76	20	16	−2	4.39
	R cerebellum	125	12	−48	−18	4.27

Additionally, MVPA results likewise revealed that activities in the DMPFC (xyz: 0, 24, 44, Z = 3.66) and DLPFC (xyz: −44, 32, 30, Z = 4.00) predicted the delay time (Figure 4i). Other brain regions included the left central operculum cortex, bilateral precentral, right frontal operculum cortex, left SPL, left PCC (Table 2). Conjunction analysis revealed overlapping regions in the DMPFC across these three types (Figure 4j), suggesting that DMPFC also represented the delay time of rewards.

3.2.3 | Distinct neural patterns in the DMPFC for the amount and delay time of future rewards

The above analyses indicated that the DMPFC represented both the amount and delay time of future rewards during intertemporal choices. We then investigated whether these neural representations were common or distinct by re-estimating the model with unsmoothed data. RSA showed low degrees of pattern similarity between the amount and delay time conditions in the DMPFC (Pearson's r value: run1 = −0.011 ± 0.118, run2 = 0.028 ± 0.098, run3 = 0.004 ± 0.078; Spearman's r value: run1 = −0.004 ± 0.121, run2 = 0.029 ± 0.108, run3 = −0.009 ± 0.081; Figure 5c). For illustration, Figure 5a shows the similarity of activity in the DMPFC across 16 levels of the amount of reward and 16 levels of delay time in one run for one subject and Figure 5b depicts the degree of pattern similarity between the amount and delay time conditions for this subject (Pearson's r = −0.015, p = .871; Spearman's r = 0.002, p = .980). Such
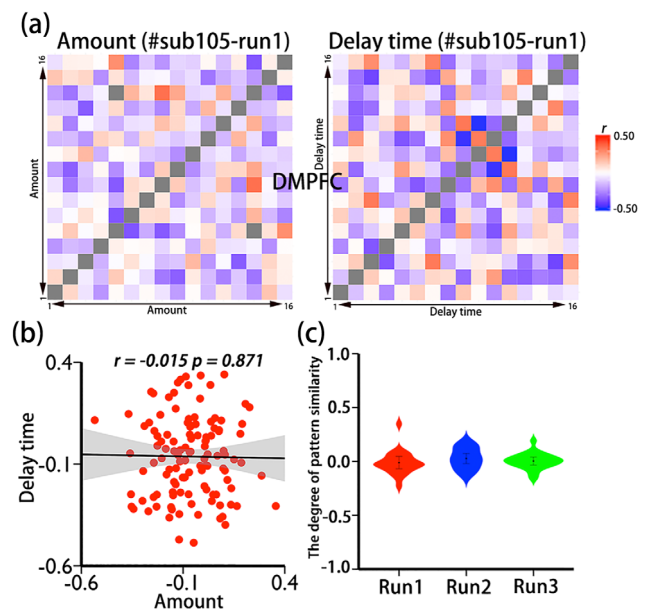

FIGURE 5 Distinct activation patterns of the amount and delay time representations in the DMPFC. The amount-related and delay-time-related representational similarities were calculated in the DMPFC (a) in one run for one subject (ID = Sub105). Scatter plots of linear correlation between the representational similarity analysis (RSA) of the amount and delay time conditions in the DMPFC (b). Violin plots of the relationships between the RSA of the amount and delay time conditions across runs and across subjects (c)

similar pattern was also observed in the remaining subjects. The above analysis suggested distinct neural patterns for the processing of the amount and delay time of future rewards.

3.2.4 | Value representations in the VMPFC, NAcc, and PCC

Previous studies have implicated the VMPFC, NAcc, and PCC in the processing of different value signals, such as the relative value (Wang et al., 2014), the subjective value (Kable & Glimcher, 2007), and the amount of delayed reward (Ballard & Knutson, 2009; Li et al., 2013). To examine specific value representations of these brain regions systematically and independently and to reduce model-selection bias, we created five simple models, which included only the task regressor, one of the five regressors [i.e., amount, subjective value (SV), decision value (DV), chosen value (CV), and summed value (SmV)]. As expected, independent models clearly showed that distinct value signals were both represented in the VMPFC (SV, *xyz*: 4, 50, −10, Z = 4.24; DV, *xyz*: 2, 58, −2, Z = 4.45; CV, *xyz*: −6, 52, −14, Z = 4.39; SmV, *xyz* = 4, 50, −10, Z = 4.24; Figure 6a). The conjunction analysis further revealed that the

overlapping brain region among these different types of value signals mainly concentrated on the VMPFC (Figure 6a). However, we found that the amount of future reward was represented in the DMPFC but not VMPFC (Figure 6a), which was consistent with the overall model. In addition, we found that the VMPFC (AM:CV:DV:SmV:SV = 0.18%:0.68%:0.36%:0.62%:0.62%), NAcc (AM:CV:DV:SmV:SV = −0.03%:0.11%:0.08%:0.08%:0.08%), and PCC (AM:CV:DV:SmV:SV = −0.03%:0.24%:0.14%:0.16%:0.16%) were modulated by all value signals but not by the amount of reward (Figure 6b). One-way ANOVA revealed that there was a significant main effect of value categories in brain signal changes in the VMPFC ($F_{[4,90]}$ = 7.659, p < .001) but not in the NAcc ($F_{[4,90]}$ = 1.564, p = .191) or in the PCC ($F_{[4,90]}$ = 1.470, p = .218). Post-hoc Bonferroni comparisons suggested that signal change of VMPFC in the Amount condition was significantly lower than CV, Summed value, and SV condition (all ps < .001). Moreover, correlational analyses further revealed that the brain signals responsible to the amount attribute were not significantly correlated with other value signals especially in the VMPFC region (all ps > 0.131; see Tables S3–S5). Collectively, these findings suggested that value signals were consistently represented in the VMPFC, NAcc, and PCC, while the amount and delay time of rewards were not processed in these brain regions.
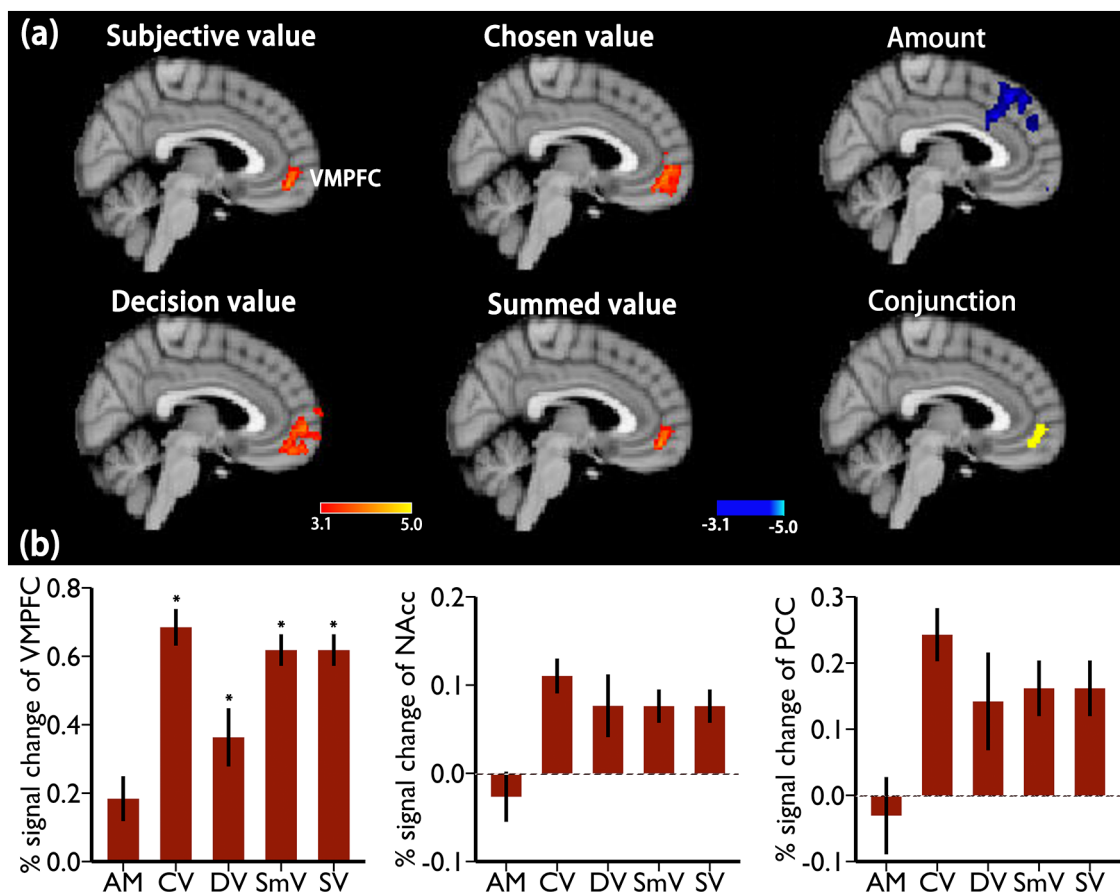

FIGURE 6 Distinct subjective values and physical attribute representation during intertemporal decision-making. (a) Different values were commonly represented in the VMPFC, including the subjective value of delayed reward, chosen value, decision value, and summed value, while the physical attribute of amount of delayed reward was independently represented in the DMPFC. Percentage signal changes for different value regressors were presented in the VMPFC, PCC, and NAcc (b). It is evident that these regions are particularly sensitive to chosen value, summed value, subjective value, but not the amount attribute

3.2.5 | Task-based functional networks related to the amount and delay time of future rewards

We used a method of representational connectivity analysis (RCA), which reflects representational strengths across different brain regions, to construct the brain networks related to the amount and delay time of future rewards. We produced the average matrices for both the amount and delay time related functional networks with AAL-90 and Power-264 parcellation scheme (Figure 7a,b). For the visual inspection of the above-mentioned matrices, all functional network matrices were displayed in a three-dimensional glass ICBM152 brain with native space, implemented by BrainNet Viewer Toolbox (Figure 7c,d; Xia, Wang, & He, 2013). These visualized matrices showed the specific connectivity patterns corresponding to the
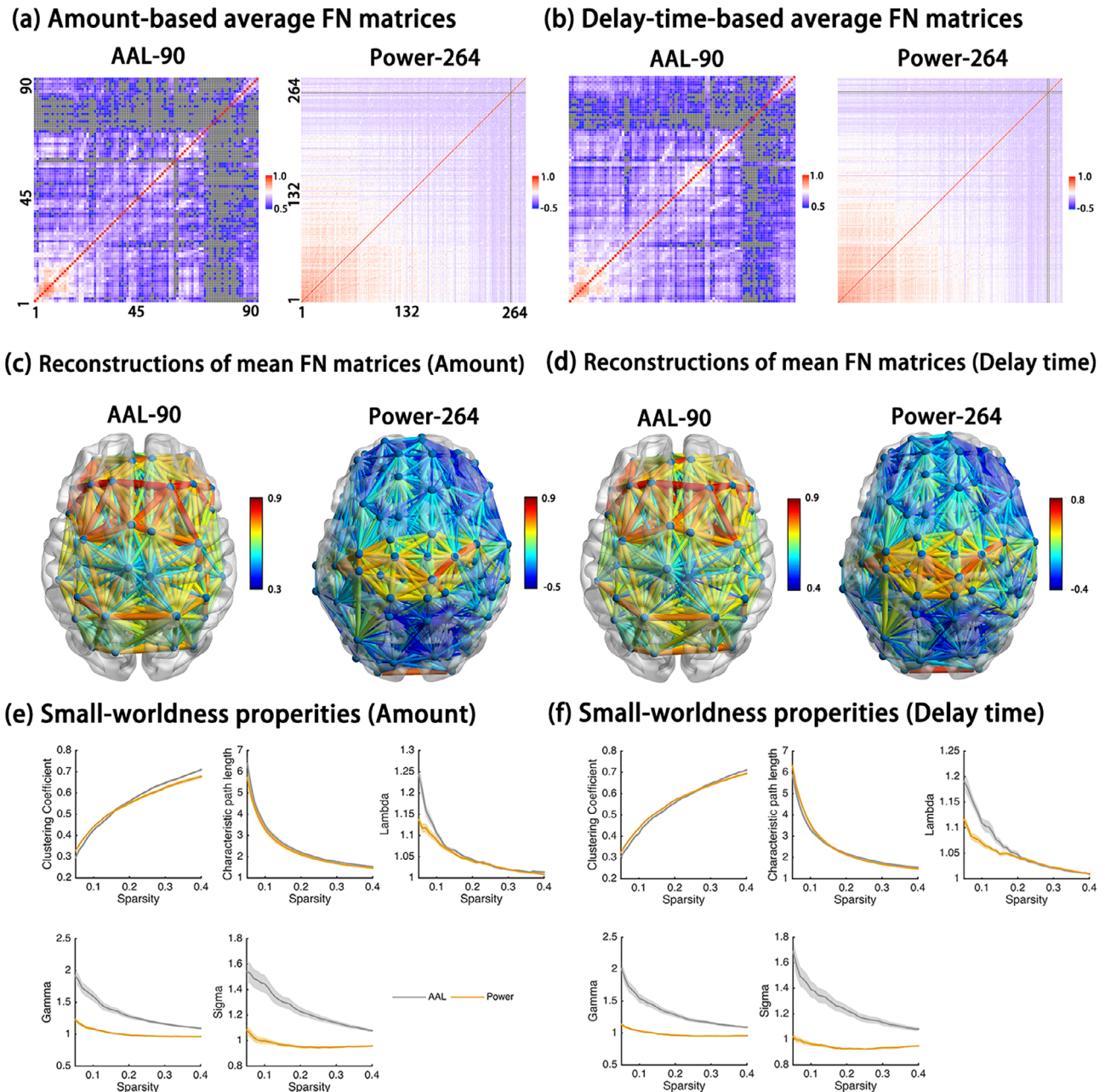

FIGURE 7 Functional connectivity matrices construction and small-world property based on representational connectivity analysis. Panel (a) represents the group-averaged functional connectivity matrices with AAL-90 and Power-264 node-defined schemes in the amount-related network. Panel (b) represents the group-averaged functional connectivity matrices with the same node-defined schemes in the delay-time-related network. Amount-related (c) and delay-time-related (d) average metrics with different atlas were reconstructed into the 3D glass brain model with ICBM-152 MNI space for visualization, respectively. The part figures (e) and (f) indicate small-world properties in the amount-related and delay-time-related functional connectome, including clustering coefficient, characteristic path length, lambda, gamma, and sigma over a range of 5–40% network sparsity in 1% increments

amount and delay time attributes across different brain regions, indicating the well-established connectivity networks (Van den Heuvel, Stam, Boersma, & Pol, 2008). After showing that the task-based network construction via RCA produced reliable brain connectomes, we proceeded to conduct graph theoretical analysis.

The small-world properties (gamma $\gamma > 1$, Lambda $\lambda \approx 1$, Sigma $\sigma > 1$) were successfully observed in both amount and delay time related networks across the range of 5–40% sparsity in low-resolution AAL-90 atlas, but not in high-resolution Power-264 atlas, especially for small-world property (Figure 7e–f; Table 4). One possible reason is that each node of high-resolution Power-264 atlas had relatively fewer voxels (only 10 mm diameter sphere), which affected the similarity matrix variation. As a result, further graph theoretical analysis only used the AAL atlas. Group-level analysis revealed that delay-discounting rate was significantly and positively correlated with path length (Lp) along all 36 thresholds (all *uncorrected p*s < .05) (Figure 8a), but negatively correlated with brain global efficiency [Eg] along the 35 thresholds (all *uncorrected ps* < 0.05) (Figure 8c) and local efficiency (Eloc) along the 21 thresholds (all *uncorrected p*s < .05) (Figure 8e) in the delay time-related network. In order to correct for multiple comparisons, we selected the area under the curve (AUC) value of topological regimes of brain connectomes (i.e., Eg, Eloc, and Lp) to link with delay discounting rates. The delay discounting rate was positively correlated with the AUC value of Lp (aLp; $r = 0.624$, $p = .004$) (Figure 8b), but negatively correlated with the AUC value of Eg (aEg; $r = -0.659$, $p = .002$) (Figure 8d) and Eloc (aEloc; $r = -0.577$, $p = .009$) (Figure 8f) in the delay time-related network. Considering the skewed distribution of k, log-transformation was further used to confirm the associations between discounting-rate and topological indexes. The results replicated the above-mentioned findings (aLp, $r = 0.494$, $p = .032$; aEg, $r = -0.588$, $p = .008$,; aEloc, $r = -0.490$, $p = .032$). Even after controlling for head motion (FD), we still observed the significant correlations between brain network properties and delay discounting rate (aEg, $r = -0.596$, $p = .009$; aEloc, $r = -0.502$, $p = .034$; aLp, $r = 0.552$, $p = .018$). However, such patterns were not observed in the amount-related network. In summary, the topological properties of
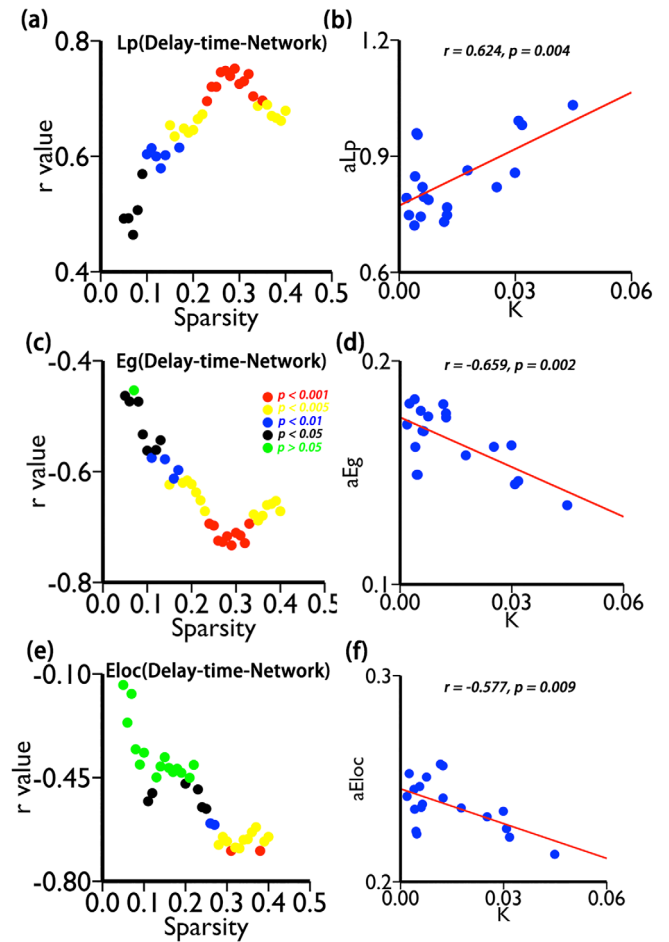

FIGURE 8 The associations between delay-time-related network properties and delay discounting rate across a network sparsity of 5–40% in 1% increments. Panel (a, c, e), respectively, indicates significant correlations of delay discounting rates with shortest path length (Lp) in the threshold of all 36-network sparsity, with global efficiency (Eg) in 35-network sparsity, and with local efficiency in 21-network sparsity. (b, d, f) Scatter plots of area under the curve value of network properties, such as aLP (b), aEg (d), and aEloc (f), as a function of discounting rate

Characteristic	Amount-network		Delay-time-network	
	Mean	SD	Mean	SD
Small-world properties				
Clustering coefficient, Creal	0.561	0.117	0.559	0.118
Characteristic path length, Lreal	2.489	1.237	2.437	1.103
Normalized C, gamma	1.323	0.305	1.319	0.310
Normalized L, lambda	1.057	0.064	1.058	0.059
Small-worldness, sigma	1.245	0.229	1.242	0.245
Efficiency properties				
Global efficiency, Eglob	0.466	0.145	0.468	0.141
Local efficiency, Eloc	0.676	0.133	0.676	0.131

TABLE 4 Group-average characteristics of amount-related and delay-time-related functional graph matrices (threshold-average) with AAL-90 atlas
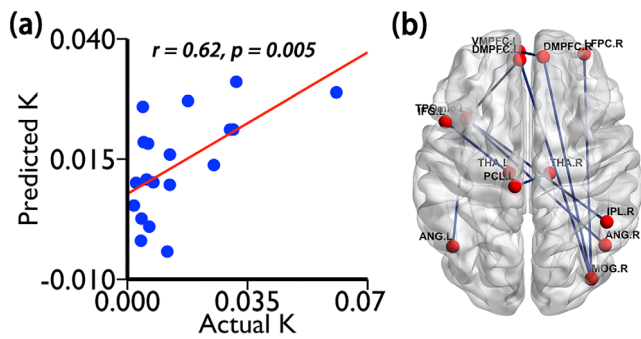
FIGURE 9 Functional connectivity model predicted discounting rate. Scatter plot shows correlation between observed delay-discounting rate and predicted delay-discounting rate by positive network and general linear model that taken into account positive network strength in amount-relevant connectome constructed via representational connectivity analysis (RCA) (a). Functional connections predicting discounting is visualized in 3D glass brain model with ICBM-152 MNI space (b)

the functional network for the delay time predicted discounting rate, but amount-related network did not.

Next, we examined whether whole-brain functional profiles of amount and delay time networks could predict delay discounting rates using connectome-based prediction model (CPM). This method is a data-driven and linear predictive model of brain-behavior relationships from connectivity data using cross-validation, which includes feature selection, feature summarization, model building, and assessment of prediction significance. We observed that delay-discounting rate was successfully predicted from amount-related functional connectivity within the positive network ($r = 0.62$, $p = .005$, 10,000-time permutation $r = 0.350$, corresponding $p < .05$; Figure 9a), but not within the negative network ($r = 0.040$, $p = .870$). Although a slightly different set of edges was selected as features in each iteration of the cross-validation, we reported all delay discounting rate-relevant edges. Figure 9b displays the connectivity of high-degree nodes, which included bilateral DMPFC, left VMPFC, right LFPC, left IFG, bilateral angular, bilateral thalamus, right IPL, left middle temporal pole (TPomid), left paracentral (PCL), and right middle occipital gyrus (MOG). These nodes by and large were found to represent the amount of reward in univariate and multivariate analyses reported earlier. However, such a prediction pattern was not observed in functional connectivity related to the processing of delay time within the positive network ($r = 0.323$, $p = .170$) and the negative network ($r = −0.261$, $p = .280$). These findings suggested that the neural activation and representational connectivity related to the amount of reward might be the primary determinant of intertemporal decision-making.

4 | DISCUSSION

The present study investigated the neural representations of the amount and delay time of future rewards during intertemporal

decision-making. Both univariate and multivariate analyses revealed that brain activity in the DMPFC and LFPC was modulated by the amount of reward whereas brain activity in the DMPFC and DLPFC was modulated by the delay time. Within the DMPFC, the two attributes of rewards showed distinct patterns of activity. In terms of individual differences, impulsive decision makers (with higher k) exhibited increased amount-related activity in the DMPFC and LFPC and decreased delay time-related activity in the DMPFC and DLPFC activation to the delay time. We further found that although the VMPFC is involved in the processing of subjective value, chosen value, relative value, and summed value, it is not involved in representing the two attributes of rewards (i.e., amount and delay time). Finally, using RCA approach, we found that topological metrics of the delay-related network (i.e., global and local efficiency) were negatively correlated with delay discounting rate, whereas whole-brain connectivity of the amount-related network was positively associated with individual's discounting rate. Taken together, our findings provided novel insights into the distributed neural representations (especially in the DMPFC) of the two attributes of future rewards, and showed the utility of using a novel network construction approach to identify topological properties related to discounting.

4.1 | Distributed neural representations of the amount attribute of delayed rewards

The univariate analysis found that the amount of future rewards was negatively correlated with the BOLD signals in the DMPFC, which replicated our previous findings in an independent sample (Wang et al., 2014). Our MVPA further confirmed that the amount of future rewards was represented in the DMPFC. Our findings were consistent with the broader literature that has identified the DMPFC as a critical brain region implicated in high-level cognitive processes during decision making, including outcome evaluation (Bush et al., 2002; Gehring & Willoughby, 2002), reward anticipation (Kahnt, Heinzle, Park, & Haynes, 2010), risk experiences (Hsu, Bhatt, Adolphs, Tranel, & Camerer, 2005; Van Duijvenvoorde et al., 2015; Xue et al., 2009), and decision-related control (Pochon, Riis, Sanfey, Nystrom, & Cohen, 2008; Van Duijvenvoorde et al., 2015). DMPFC has been also considered critical for cognitive control, with consistent evidence of activation in tasks related to involving conflict and strategic control (Botvinick, Nystrom, Fissell, Carter, & Cohen, 1999). Furthermore, the DMPFC studies which used both univariate and multivariate pattern analyses found that this region also represented the potential gains during risky decision-making (Jimura & Poldrack, 2012; Tom et al., 2007). Multivariate analysis also showed that DMPFC is involved in the emotion-related perception with high decoding accuracy (Jastorff, Huang, Giese, & Vandenbulcke, 2015; Kim et al., 2015). Thus, this region has become one of the high-efficiency target sites of noninvasive treatment via repetitive transcranial magnetic stimulation for reward/emotion-related disorders like major depression disorder (MDD) (Downar et al., 2014; Salomons et al., 2014) and posttraumatic stress disorder (PTSD) (Woodside et al., 2017).

However, some prior studies reported that the VMPFC but not DMPFC was involved in the processing of the amount of future rewards (Ballard & Knutson, 2009; Li et al., 2013). There are two potential reasons for this inconsistency. The first is that our study includes a wider range of the amounts of future rewards (i.e., 16 levels vs. 7 levels in previous studies), which may provide a greater power to detect amount-related activity in the DMPFC. The other explanation is that our independent manipulations of the amount and delay time helped clarified the contributions of the DMPFC. Additionally, there is extensive evidence supporting the functional and structural coupling between DMPFC and VMPFC, a region associated with value integration, emotional experiences, and self-processing (Koush et al., 2019; Kuzmanovic, Rigoux, & Tittgemeyer, 2018). Such objective amount representation and subjective amount processing might reflect complex neural mechanisms of inter-temporal choices at different stages of decisions. Furthermore, the subjective amount process is difficult to separate from other value signals such as relative value, chosen value, and summed value due to the low temporal resolution.

4.2 | Distributed neural representations of the delay-time attribute of delayed rewards

On both univariate and multivariate analyses found that the DLPFC is one of key regions that represent the delay time attribute. This finding was consistent with prior univariate studies (Ballard & Knutson, 2009; Li et al., 2013). Delay time is an important attribute taken into account when people make inter-temporal choices, and largely determines the subjective value computed by this attribute and reward amount information (Ainslie, 1975). In general, the time attribute is viewed as a cost and has been attracting attention in neuroeconomics and econophysics combined with a variety of computational models (Takahashi, Oono, & Radford, 2008). Recent studies have also demonstrated be predictive of this attribute on the individual's actual choices based on eye tracking technique (Amasino, Sullivan, Kranton, & Huettel, 2019), which is summarized as the attribute-wise choice theory. Functional MRI studies have suggested the involvement of prefrontal cortex in the time perception, including the DLPFC and DMPFC (Pouthas et al., 2005), which are also involved in the inter-temporal choices (Peters & Buchel, 2010). Prior evidence has pointed out that long delays might reduce activations in reward-magnitude-related regions (Kable & Glimcher, 2007), elicit activations in uncertainty-related regions (Preuschoff, Quartz, & Bossaerts, 2008), and require cognitive control and inhibition of prepotent responses such as DLPFC, IFG, and posterior parietal cortex (Aron, Fletcher, Bullmore, Sahakian, & Robbins, 2003; McClure et al., 2004) when waiting for a larger future reward. Although there are suggestive evidence of top-down control processes instantiated in the DLPFC via connections with the DLPFC with VMPFC, NAcc, and PCC (Figner et al., 2010; Peters & Büchel, 2011; Steinbeis, Haushofer, Fehr, & Singer, 2016; Wang et al., 2016), researchers are still debating about the precise functional role of the DLPFC in intertemporal decision-making and how it may differ across different decision stages (Figner et al., 2010; Luo, Ainslie, Giragosian, & Monterosso, 2009; Peters & Büchel, 2011).

In addition to the DLPFC region, our MVPA also showed that the delay time was represented in the DMPFC. This finding was consistent with prior univariate studies (Li et al., 2013) and structural imaging studies (Beagle et al., 2020; Massar et al., 2015). Prior behavioral studies have observed the intimate associations between subjective time perception and delay discounting (Takahashi et al., 2008). If delays are subjectively perceive longer than they actually are, individuals might more prefer to choose smaller but sooner rewards. Previous imaging studies also have implicated the critical role of the DMPFC, a functionally defined region that is overlapping with the pre-SMA and dorsal ACC (Addis & Schacter, 2008; Buckner & Carroll, 2007), on the episodic prospection and predictive of far-sighted choices before making decisions (Benoit, Gilbert, & Burgess, 2011; Peters & Buchel, 2010) possibly via familiarity (Sasse, Peters, Büchel, & Brassen, 2015). Subjects who were more sensitive to the delay time exhibited decreased activity in the DMPFC (Ballard & Knutson, 2009; Li et al., 2013). Individual differences in temporal preferences were associated with the ability of episodic thinking of future events (Peters & Büchel, 2011). The present study not only replicates the prior findings, but also suggests a distributed neural coding of such region to delay attribute of future rewards.

4.3 | Brain activities and network properties responsible to the amount and delay time predict discounting rate

Our individual differences analyses also showed close associations between brain responses to the amount and delay time of future rewards and discounting rates, consistent with previous studies (Ballard & Knutson, 2009). Impulsive decision makers are generally characterized by hyperactivation in the valuation when responding to immediate rewards but hypoactivation in the cognitive control network and prospection network (Figner et al., 2010; Hariri et al., 2006; McClure et al., 2004). Similarly, we found increased neural activity in valuation network in response to the amount of future rewards and decreased neural activation in the prospection network or cognitive control (especially the DLPFC and DMPFC) in response to the delay time. There is also converging evidence from morphological (i.e., gray matter volume and thickness) and functional connectivity studies (i.e., regional homogeneity, activation level, couplings with other regions, and activation patterns in risky decisions) that the DMPFC is related to delay discounting (Beagle et al., 2020; Lv et al., 2019; Lv, Wang, Chen, Xue, & He, 2020; Sripada et al., 2011; Wang et al., 2016). A recent study found the independent contributions of amount and delay time on individual's choices combined with behavioral analyses, computational models and eye tracking measures (Amasino et al., 2019), which supports the attributed-wise choice pattern compared with option-wise pattern. Consistent with this view,

our functional imaging findings further confirmed the independent role of these two attributes of future rewards via multivariate pattern analysis and RSA. Together with previous studies, our study results further suggested that the DMPFC-related attributes representations play a crucial role in impulsive behaviors.

Using representational connectivity analysis, our study constructed brain networks for the representations of the amount and delay time. Considerable evidence from multiple-modalities brain data has consistently implicated that human brain is a highly integrated network system, manifesting a small-world organization via graph theoretical analysis (Sporns, 2010; Van den Heuvel, Kahn, Goni, & Sporns, 2012). For this organization, it is widely characterized by greater cliquishness but relatively shorter path length. Such features were consistently observed in the amount/time-related representational networks, irrespective of which parcellation scheme was conducted in present study. In general, the small-world organization is inevitably associated with parallel information processing, which in large determines the efficiency of both local and global high-order cognitive communication (Bassett & Bullmore, 2017). Interestingly, we found that the delay-time-related network's efficiency (the shortest path length, global efficiency, and local efficiency) was negatively correlated with discounting rates. In other words, individuals with low efficiency in their processing of the delay time were more impulsive. Network efficiency is a critical index used to estimate the brain's capability of information separation and integration (Sporns, 2010; Van den Heuvel et al., 2012), and has been shown to be significantly associated with impulsivity (Chen et al., 2019; Wang, Lv, et al., 2020a). Although such association between brain efficiency and discounting-rate was also found in traditional network constructed based on the resting-state fMRI data (Chen et al., 2019; Wang, Zhu, et al., 2020b), it is the first work to compute the specific-attribute functional topological metrics and make a prediction on behavioral performance in present study. Such network construction indeed provides some special principles of brain neural representational organization, which cannot be probed based on the strategy of traditional network construction. Collectively, our findings further demonstrated the important role of network efficiency supporting specific reward attributes in intertemporal decisions (Peters & Büchel, 2011).

Similarly, connetome-based characteristics were also found to be associated with the amount of rewards in which the critical functional connectivity predominantly distributed on brain regions responsible for amount attribute. Combined with the prediction of the delay-related network efficiency, amount and delay time might independently determines the individual's behavioral performances such as choices and discounting rate, manifesting as distinct brain patterns such as network efficiency and functional connectivity strength. It is consistent with recent attribute-wise choice theory that highlights separated roles of amount and delay time in the intertemporal choices from the perspective of behavioral analyses, computational model and eye tracking technique (Amasino et al., 2019). Furthermore, connectome-based functional connectivity was composed of the connectivity of the hub amount-related area (i.e., DMPFC) with other

brain regions such as visual, ventral prefrontal, and parietal cortex. The functional communications among these regions might reflect the integral processes of decisions, including visual information input, parietal cognitive control, and their modulations on reward processing (i.e., DMPFC, LFPC, and VMPFC). Taken together, the separated distributed neural representation of amount and delay time and corresponding prediction on individual differences further provide the brain functional supports for attribute-wise choice theory, which suggests novel neural mechanisms underlying human inter-temporal choices.

4.4 | Neural mechanisms underlying representation of physical attributes and subjective computation

The physical attributes of future rewards such as amount of reward and delay time were represented in the DMPFC with distinct activation patterns via RSA. It is consistent with recent study that found separable processing for amount and time information but not integrated processing via drift diffusion model combined with eye tracking measures (Amasino et al., 2019). Such attribute-wise manner is largely not predicted based on the traditional option-wise comparison pattern, which emphasizes the integrated option of these two attributes. Furthermore, amount and time information has different contributions to individual differences in intertemporal choice, which was also observed in our individual differences analysis, manifesting as positive prediction of amount-related brain responses and negative prediction of time-related brain responses on discounting rate. However, individual differences with higher subjective value in the VMPFC were not directly associated with individual variability in the discounting rate, which might support the attribute-wise decision processing not option-wise processing during intertemporal choice.

The present study indicates that several value signals such as the subjective value, chosen value, summed value, and relative value, both were represented in the VMPFC, one critical area processing value-related information that wisely demonstrated in the fMRI studies (Kable & Glimcher, 2007; Wang et al., 2014). Due to the fixed immediate option manipulation, these value signals might exhibit a collinearity issue, which did not identify the precise function of VMPFC in decision stage in our study. Indeed, VMPFC has been demonstrated to process the relative value (Wang et al., 2014), chose value, and subjective value in several discounting-related studies (Kable & Glimcher, 2007; Li et al., 2013).

4.5 | Strengths and limitations

The present study features several novel strengths. This study is the first work to examine parametric variations in amount and delay time estimation combined with univariate and multivariate pattern analysis. The amount and delay time were independently manipulated to distinguish the mental processes responsible for these two attributes.

Furthermore, individual differences analysis and novel RCA-based graph-theoretical analysis both showed consistent patterns and provided cross-validation, which improve the confidence of make a conclusion. Compared with univariate analysis, multivariate analysis further extends our understanding of the neural representations of physical attributes of delayed rewards on medial and lateral PFC with distributed coding pattern. Furthermore, physical attribute-based network reconstruction indeed carries on the specific topological information used to predict individual's performance.

Beyond the benefits conferred by the present design, there are several limitations. Firstly, the sample size is relative small and might influence the generalization of our findings in a larger population. Recently, a number of studies have systematically investigated the possible influence of sample size on stability and interpretation of brain–behavior correlations in task-based fMRI data (Braver, Cole, & Yarkoni, 2010; Dubois & Adolphs, 2016; Grady, Rieck, Nichol, & Rodrigue, 2021). In order to further increase the robustness of our results, different strategies were used for the cross-validation, including strictly statistical power, permutation test, and controlling of confounding factors. Secondly, due to the fixed immediate option, it is difficult to separate neural responses to distinct value signals such as the subjective value, chosen value, summed value, and relative value because of the issue of collinearity. Thirdly, non-neural related signals (i.e., respiration and pulse) are potential factors that might impact the connectivity analysis, which further needs to be taken into account in future study in order to exclude their impacts.

4.6 | Conclusion

The present study examined neural representations (especially in the DMPFC) of the amount and delay time of rewards during intertemporal decision-making, and identified brain networks for those representations. Together with prior studies, our results support a ventral-dorsal dissociation of MFPC in neural representations of values (e.g., subjective values and relative value) and attributes of the reward (i.e., amount and delay time); RCA-based network construction is reliable and carries on specific topological information used to predict individual variations in behavioral task. These findings provide novel insights into the neural representations of amount and delay attribute, and support attribute-wise processing during intertemporal decision-making.

CONFLICT OF INTEREST

The authors declare no conflicts of interest.

AUTHOR CONTRIBUTION

Qiang Wang: Developed the study concept and design. **Pinchun Wang, Yajie Wang, Manman Zhang, Yuxuan Zhu, and Shiyu Wei:** Performed the data collection. **Qiang Wang, Pinchun Wang, Maomiao Peng, and Yajie Wang:** Performed the data analysis and interpretation under the supervision of Xuejun Bai; **Qiang Wang, Pinchun Wang, Shan Luo, and Chuansheng Chen:** Drafted the manuscript; **Xuejun Bai, Chuansheng Chen, and Shan Luo:** Provided critical revisions. All the authors approved the final manuscript for submission.

DATA AVAILABILITY STATEMENT

The data that support the findings of this study are available from the Functional MRI Center at Tianjin Normal University (TJNU). Data and code are available from the corresponding authors with the permission of the TJNU.

ORCID

Qiang Wang https://orcid.org/0000-0002-1081-6690

REFERENCES

Addis, D. R., & Schacter, D. L. (2008). Constructive episodic simulation: Temporal distance and detail of past and future events modulate hippocampal engagement. *Hippocampus*, *18*(2), 227–237. https://doi.org/10.1002/hipo.20405

Ainslie, G. (1975). Specious reward: A behavioral theory of impulsiveness and impulsive control. *Psychological Bulletin*, *82*(4), 463–496.

Alessi, S., & Petry, N. M. (2003). Pathological gambling severity is associated with impulsivity in a delay discounting procedure. *Behavioural Processes*, *64*(3), 345–354. https://doi.org/10.1016/S0376-6357(03)00150-5

Amasino, D. R., Sullivan, N. J., Kranton, R. E., & Huettel, S. A. (2019). Amount and time exert independent influences on intertemporal choice. *Nature Human Behaviour*, *3*, 383–392.

Aron, A. R., Fletcher, P. C., Bullmore, E., Sahakian, B. J., & Robbins, T. W. (2003). Stop-signal inhibition disrupted by damage to right inferior frontal gyrus in humans. *Nature Neuroscience*, *6*, 115–116. https://doi.org/10.1038/nn1003

Ballard, K., & Knutson, B. (2009). Dissociable neural representations of future reward magnitude and delay during temporal discounting. *Neuroimage*, *45*(1), 143–150. https://doi.org/10.1016/j.neuroimage.2008.11.004

Bassett, D. S., & Bullmore, E. (2017). Small-world brain networks revisited. *The Neuroscientist*, *23*(5), 499–516. https://doi.org/10.1177/1073858416667720

Beagle, A. J., Zahir, A., Borzello, M., Kayser, A. S., Hsu, M., Miller, B. L., … Chiong, W. (2020). Amount and delay insensitivity during intertemporal choice in three neurodegenerative diseases reflects dorsomedial prefrontal atrophy. *Cortex*, *124*, 54–65. https://doi.org/10.1016/j.cortex.2019.10.009

Benoit, R. G., Gilbert, D. T., & Burgess, P. W. (2011). A neural mechanism mediating the impact of episodic prospection on farsighted decisions. *The Journal of Neuroscience*, *31*(18), 6771–6779. https://doi.org/10.1523/JNEUROSCI.6559-10.2011

Bickel, W. K., Odum, A. L., & Madden, G. J. (1999). Impulsivity and cigarette smoking: Delay discounting in current, never, and ex-smokers. *Psychopharmacology*, *146*(4), 447–454. https://doi.org/10.1007/PL00005490

Botvinick, M., Nystrom, L. E., Fissell, K., Carter, C. S., & Cohen, J. D. (1999). Conflict monitoring versus selection-for-action in anterior cingulate cortex. *Nature*, *402*, 179–181. https://doi.org/10.1038/46035

Braver, T. S., Cole, M. W., & Yarkoni, T. (2010). Vive les differences! Individual variation in neural mechanisms of executive control. *Current Opinion in Neurobiology*, 20(2), 242–250. https://doi.org/10.1016/j.conb.2010.03.002

Buckner, R. L., & Carroll, D. C. (2007). Self-projection and the brain. *Trends in Cognitive Sciences*, 11(2), 49–57. https://doi.org/10.1016/j.tics.2006.11.004

Bullmore, E. T., & Bassett, D. S. (2011). Brain graphs: Graphical models of the human brain connectome. *Annual Review of Clinical Psychology*, 7, 113–140. https://doi.org/10.1146/annurev-clinpsy-040510-143934

Bush, G., Vogt, B. A., Holmes, J., Dale, A. M., Greve, D., Jenike, M. A., & Rosen, B. R. (2002). Dorsal anterior cingulate cortex: A role in reward-based decision making. *Proceedings of the National Academy of Sciences*, 99(1), 523–528. https://doi.org/10.1073/pnas.012470999

Cai, H., Chen, J., Liu, S., Zhu, J., & Yu, Y. (2020). Brain functional connectome-based prediction of individual decision impulsivity. *Cortex*, 125, 288–298. https://doi.org/10.1016/j.cortex.2020.01.022

Chen, Z., Hu, X., Chen, Q., & Feng, T. (2019). Altered structural and functional brain network overall organization predict human intertemporal decision-making. *Human Brain Mapping*, 40(1), 306–328. https://doi.org/10.1002/hbm.24374

Dale, A. M. (1999). Optimal experimental design for event-related fMRI. *Human Brain Mapping*, 8(2), 109–114. https://doi.org/10.1002/(SICI)1097-0193(1999)8:2/3%3C109::AID-HBM7%3E3.3.CO;2-N

Downar, J., Geraci, J., Salomons, T. V., Dunlop, K., Wheeler, S., McAndrews, M. P., ... Giacobbe, P. (2014). Anhedonia and reward-circuit connectivity distinguish nonresponders from responders to dorsomedial prefrontal repetitive transcranial magetic stimulation in major depression. *Biological Psychiatry*, 76(3), 176–185.

Drucker, H., Burges, C. J., Kaufman, L., Smola, A. J., & Vapnik, V. (1997). Support vector regression machines. *Paper presented at the Advances in neural information processing systems*. 28(7):779–784.

Dubois, J., & Adolphs, R. (2016). Building a science of individual differences from fMRI. *Trends in Cognitive Sciences*, 20(6), 425–443. https://doi.org/10.1016/j.tics.2016.03.014

Figner, B., Knoch, D., Johnson, E. J., Krosch, A. R., Lisanby, S. H., Fehr, E., & Weber, E. U. (2010). Lateral prefrontal cortex and self-control in intertemporal choice. *Nature Neuroscience*, 13(5), 538. https://doi.org/10.1038/nn.2516

Friston, K., Penny, W., & Glaser, D. (2005). Conjunction revisited. *Neuroimage*, 25(3), 661–667. https://doi.org/10.1016/j.neuroimage.2005.01.013

Gehring, W. J., & Willoughby, A. R. (2002). The medial frontal cortex and the rapid processing of monetary gains and losses. *Science*, 295(5563), 2279–2282. https://doi.org/10.1126/science.1066893

Grady, C. L., Rieck, J. R., Nichol, D., & Rodrigue, K. M. (2021). Influence of sample size and analytic approach on stability and interpretation of brain-behavior correlations in task-related fMRI data. *Human Brain Mapping*, 2021(42), 204–219.

Green, L., & Myerson, J. (1996). Exponential versus hyperbolic discounting of delayed outcome: Risk and waiting time. *American Zoologist*, 36(4), 496–505.

Green, L., & Myerson, J. (2004). A discounting framework for choice with delayed and probabilistic rewards. *Psychological Bulletin*, 130(5), 769–792. https://doi.org/10.1037/0033-2909.130.5.769

Hanke, M., Halchenko, Y. O., Sederberg, P. B., Hanson, S. J., Haxby, J. V., & Pollmann, S. (2009). PyMVPA: A python toolbox for multivariate pattern analysis of fMRI data. *Neuroinformatics*, 7, 37–53. https://doi.org/10.1007/s12021-008-9041-y

Hariri, A. R., Brown, S. M., Williamson, D. E., Flory, J. D., de Wit, H., & Manuck, S. B. (2006). Preference for immediate over delayed rewards is associated with magnitude of ventral striatal activity. *Journal of Neuroscience*, 26(51), 13213–13217. https://doi.org/10.1523/JNEUROSCI.3446-06.2006

Hsu, M., Bhatt, M., Adolphs, R., Tranel, D., & Camerer, C. F. (2005). Neural systems responding to degrees of uncertainty in human decision-making. *Science*, 310(5754), 1680–1683. https://doi.org/10.1126/science.1115327

Jastorff, J., Huang, Y.-A., Giese, M. A., & Vandenbulcke, M. (2015). Common neural correlates of emotion perception in humans. *Human Brain Mapping*, 36(10), 4184–4201. https://doi.org/10.1002/hbm.22910

Jenkinson, M., & Smith, S. M. (2001). A global optimisation method for robust affine registration of brain images. *Medical Image Analysis*, 5(2), 143–156. https://doi.org/10.1016/S1361-8415(01)00036-6

Jimura, K., & Poldrack, R. A. (2012). Analyses of regional-average activation and multivoxel pattern information tell complementary stories. *Neuropsychologia*, 50(4), 544–552. https://doi.org/10.1016/j.neuropsychologia.2011.11.007

Kable, J. W., & Glimcher, P. W. (2007). The neural correlates of subjective value during intertemporal choice. *Nature Neuroscience*, 10(12), 1625. https://doi.org/10.1038/nn2007

Kable, J. W., & Glimcher, P. W. (2009). The neurobiology of decision: Consensus and controversy. *Neuron*, 63(6), 733–745. https://doi.org/10.1016/j.neuron.2009.09.003

Kahnt, T. (2018). A decade of decoding reward-related fMRI signals and where we go from here. *Neuroimage*, 180, 324–333. https://doi.org/10.1016/j.neuroimage.2017.03.067

Kahnt, T., Heinzle, J., Park, S. Q., & Haynes, J.-D. (2010). The neural code of reward anticipation in human orbitofrontal cortex. *Proceedings of the National Academy of Sciences*, 107(13), 6010–6015. https://doi.org/10.1073/pnas.0912838107

Kim, J., Schultz, J., Rohe, T., Wallraven, C., Lee, S.-W., & Bulthoff, H. H. (2015). Abstract representations of associated emotions in the human brain. *The Journal of Neuroscience*, 35(14), 5655–5663. https://doi.org/10.1523/JNEUROSCI.4059-14.2015

Koush, Y., Pichon, S., Eickhoff, S. B., Van De Ville, D., Vuilleumier, P., & Sharnowski, F. (2019). Brain networks for engaging oneself in positive-social emotion regulation. *Neuroimage*, 189, 106–115. https://doi.org/10.1016/j.neuroimage.2018.12.049

Kriegeskorte, N., Mur, M., & Bandettini, P. (2008). Representational similarity analysis-connecting the branches of systems neuroscience. *Frontiers in Systems Neuroscience*, 2, 1–28.

Kuzmanovic, B., Rigoux, L., & Tittgemeyer, M. (2018). Influence of vmPFC on dmPFC predicts valence-guided belief formation. *The Journal of Neuroscience*, 38(37), 7996–8010. https://doi.org/10.1523/JNEUROSCI.0266-18.2018

Li, N., Ma, N., Liu, Y., He, X.-S., Sun, D.-L., Fu, X.-M., ... Zhang, D. R. (2013). Resting-state functional connectivity predicts impulsivity in economic decision-making. *Journal of Neuroscience*, 33(11), 4886–4895. https://doi.org/10.1523/JNEUROSCI.1342-12.2013

Luo, S., Ainslie, G., Giragosian, L., & Monterosso, J. R. (2009). Behavioral and neural evidence of incentive bias for immediate rewards relative to preference-matched delayed rewards. *Journal of Neuroscience*, 29(47), 14820–14827. https://doi.org/10.1523/JNEUROSCI.4261-09.2009

Lv, C., Wang, Q., Chen, C., Qiu, J., Xue, G., & He, Q. (2019). The regional homogeneity patterns of the dorsal medial prefrontal cortex predict individual differences in decision impulsivity. *Neuroimage*, 200, 556–561. https://doi.org/10.1016/j.neuroimage.2019.07.015

Lv, C., Wang, Q., Chen, C., Xue, G., & He, Q. (2020). Activation patterns of the dorsal medial prefrontal cortex and frontal pole predict individual differences in decision impulsivity. *Brain Imaging and Behavior*, 15, 421–429. https://doi.org/10.1007/s11682-020-00270-1

Massar, S. A., Libedinsky, C., Chee, W., Huettel, S. A., & Chee, M. W. (2015). Separate and overlapping brain areas encode subjective value during delay and effort discounting. *Neuroimage*, 120, 104–113. https://doi.org/10.1016/j.neuroimage.2015.06.080

McClure, S. M., Laibson, D. I., Loewenstein, G., & Cohen, J. D. (2004). Separate neural systems value immediate and delayed monetary rewards. *Science*, 306(5695), 503–507. https://doi.org/10.1126/science.1100907

Misaki, M., Kim, Y., Bandettini, P., & Kriegeskorte, N. (2010). Comparison of multivariate classifiers and response normalizations for pattern-information fMRI. *Neuroimage*, 53(1), 103–118. https://doi.org/10.1016/j.neuroimage.2010.05.051

Mumford, J. A. (2007). A guide of calculating percent change with Featquery: Unpublished tech report. Retrieved from http://mumford.bol.ucla.edu/perchange_guide.pdf.

Paloyelis, Y., Asherson, P., Mehta, M. A., Faraone, S. V., & Kuntsi, J. (2010). DAT1 and COMT effects on delay discounting and trait impulsivity in male adolescents with attention deficit/hyperactivity disorder and healthy controls. *Neuropsychopharmacology*, 35(12), 2414. https://doi.org/10.1038/npp.2010.124

Peters, J., & Buchel, C. (2010). Episodic future thinking reduces reward delay discounting through an enhancement of prefrontal-Mediotemporal interactions. *Neuron*, 66, 138–148. https://doi.org/10.1016/j.neuron.2010.03.026

Peters, J., & Büchel, C. (2011). The neural mechanisms of inter-temporal decision-making: Understanding variability. *Trends in Cognitive Sciences*, 15(5), 227–239. https://doi.org/10.1016/j.tics.2011.03.002

Pochon, J., Riis, J., Sanfey, A. G., Nystrom, L. E., & Cohen, J. D. (2008). Functional imaging of decision conflict. *The Journal of Neuroscience*, 28(13), 3468–3473. https://doi.org/10.1523/JNEUROSCI.4195-07.2008

Pouthas, V., George, N., Poine, J.-B., Pfeuty, M., VandeMoorteele, P.-F., Hugueville, L., ... Renault, B. (2005). Neural network involved in time perception: An fMRI study comparing long and short interval estimation. *Human Brain Mapping*, 25(4), 433–441. https://doi.org/10.1002/hbm.20126

Preuschoff, K., Quartz, S. R., & Bossaerts, P. (2008). Human insula activation reflects risk prediction errors as well as risk. *The Journal of Neuroscience*, 28(11), 2745–2752. https://doi.org/10.1523/JNEUROSCI.4286-07.2008

Rangel, A., Camerer, C. F., & Montague, P. R. (2008). A framework for studying the neurobiology of value-based decision making. *Nature Reviews Neuroscience*, 9, 545–556. https://doi.org/10.1038/nrn2357

Ritchie, J. B., Kaplan, D. M., & Klein, C. (2019). Decoding the brain: Neural representation and the limits of multivariate pattern analysis in cognitive neuroscience. *The British Journal for the Philosophy of Science*, 70(2), 581–607. https://doi.org/10.1093/bjps/axx023

Rubinov, M., Knock, S. A., Stam, C., Sifis, M., Harris, A. W., Williams, L. M., & Breakspear, M. (2009). Small-world properities of nonlinear brain activity in schizophrenia. *Human Brain Mapping*, 30(2), 403–416. https://doi.org/10.1002/hbm.20517

Rudie, J., Brown, J., Beck-Pancer, D., Hernandez, L., EL, D., Thomas, P., ... Dapretto, M. (2013). Altered functional and structural brain network organization in autism. *Neuroimage: Clinical*, 2, 79–94. https://doi.org/10.1016/j.nicl.2012.11.006

Salomons, T. V., Dunlop, K., Kennedy, S. H., Flint, A., Geraci, J., Giacobbe, P., & Downar, J. (2014). Resting-state cortico-thalamic-striatal connectivity predicts response to dorsomedial prefrontal rTMS in major depressive disorder. *Neuropsychopharmacology*, 39, 488–498. https://doi.org/10.1038/npp.2013.222

Samuelson, P. A. (1937). A note on measurement of utility. *The Review of Economic Studies*, 4(2), 155–161.

Sasse, L. K., Peters, J., Büchel, C., & Brassen, S. (2015). Effects of prospective thinking on intertemporal choice: The role of familiarity. *Human Brain Mapping*, 36(10), 4210–4221. https://doi.org/10.1002/hbm.22912

Shen, X., Finn, E. S., Scheinost, D., Rosenberg, M. D., Chun, M. M., Papademetris, X., & Constable, R. T. (2017). Using connectome-based predictive modeling to predict individual behavor from brain connectivity. *Nature Protocols*, 12, 506–518. https://doi.org/10.1038/nprot.2016.178

Sporns, O. (2010). *Networks of the brain*. Cambridge, MA: MIT Press.

Sripada, C. S., Gonzalez, R., Phan, K. L., & Liberzon, I. (2011). The neural correlates of intertemporal decision-making: Contributions of subjective value, stimulus type, and trait impulsivity. *Hum Brain Mapping*, 32(10), 1637–1648. https://doi.org/10.1002/hbm.21136

Steinbeis, N., Haushofer, J., Fehr, E., & Singer, T. (2016). Development of behavioral control and associated vmPFC-DLPFC connectivity explains children's increased resistance to temptation in Intertemporal choice. *Cerebral Cortex*, 26(1), 32–42. https://doi.org/10.1093/cercor/bhu167

Takahashi, T., Oono, H., & Radford, M. H. (2008). Psychophysics of time perception and intertemporal choice models. *Physcia A: Statistical Mechanics and its Applications*, 387(8-9), 2066–2074. https://doi.org/10.1016/j.physa.2007.11.047

Tom, S. M., Fox, C. R., Trepel, C., & Poldrack, R. A. (2007). The neural basis of loss aversion in decision-making under risk. *Science*, 315(5811), 515–518. https://doi.org/10.1126/science.1134239

Van den Heuvel, M., Kahn, R. S., Goni, J., & Sporns, O. (2012). High-cost, high-capacity backbone for global brain communication. *Proceedings of the National Academy of Sciences*, 109(28), 11372–11377. https://doi.org/10.1073/pnas.1203593109

Van den Heuvel, M., Stam, C., Boersma, M., & Pol, H. H. (2008). Small-world and scale-free organization of voxel-based resting-state functional connectivity in the human brain. *Neuroimage*, 43(3), 528–539. https://doi.org/10.1016/j.neuroimage.2008.08.010

Van Duijvenvoorde, A. C., Huizenga, H. M., Somerville, L. H., Delgado, M. R., Powers, A., Weeda, W. D., ... Figner, B. (2015). Neural correlates of expected risks and returns in risky choice across development. *The Journal of Neuroscience*, 35(4), 1549–1560. https://doi.org/10.1523/JNEUROSCI.1924-14.2015

Wang, J., Wang, X., Xia, M., Liao, X., Evans, A., & He, Y. (2015). GRETNA: A graph theoretical network analysis toolbox for imaging connectomics. *Frontiers in Human Neuroscience*, 9, 386. https://doi.org/10.3389/fnhum.2015.00386

Wang, Q., Chen, C., Cai, Y., Li, S., Zhao, X., Zheng, L., ... Xue, G. (2016). Dissociated neural substrates underlying impulsive choice and impulsive action. *Neuroimage*, 134, 540–549. https://doi.org/10.1016/j.neuroimage.2016.04.010

Wang, Q., Luo, S., Monterosso, J., Zhang, J., Fang, X., Dong, Q., & Xue, G. (2014). Distributed value representation in the medial prefrontal cortex during intertemporal choices. *Journal of Neuroscience*, 34(22), 7522–7530. https://doi.org/10.1523/JNEUROSCI.0351-14.2014

Wang, Q., Lv, C., He, Q., & Xue, G. (2020a). Dissociable fronto-striatal functional networks predict choice impulsivity. *Brain Structure and Function*, 225(8), 2377–2386. https://doi.org/10.1007/s00429-020-02128-0

Wang, Q., Wei, S., Im, H., Zhang, M., Wang, P., Zhu, Y., ... Bai, X. (2021). Neuroanatomical and functional substrates of the greed personality trait. *Brain Structure and Function*, 1–12.

Wang, Q., Zhu, Y., Wang, Y., Chen, C., He, Q., & Xue, G. (2020b). Intrinsic non-hub connectivity predicts human inter-temporal decision-making. *Brain Imaging and Behavior*, 1–12. https://doi.org/10.1007/s11682-020-00395-3

Woodside, D. B., Colton, P., Lam, E., Dunlop, K., Rzeszutek, J., & Downar, J. (2017). Dorsomedial prefrontal cortex repetitive transcranial magnetic stimulation treatment of posttraumatic stress disorder in eating disorders: An open-label case series. *Eating Disorders*, 50(10), 1231–1234. https://doi.org/10.1002/eat.22764

Xia, M., Wang, J., & He, Y. (2013). BrainNet viewer: A network visualization tool for human brain connectomics. *PLoS One*, 8(7), e68910. https://doi.org/10.1371/journal.pone.0068910

Xue, G., Lu, Z.-L., Levin, I. P., Weller, J. A., Li, X., & Antoine, B. (2009). Functional dissociations of risk and reward processing in the medial prefrontal cortex. *Cerebral Cortex*, *19*(5), 1019–1027. https://doi.org/10.1093/cercor/bhn147

Zha, R., Bu, J., Wei, Z., Han, L., Zhang, P., Ren, J., … Zhang, X. (2019). Transforming brain signals related to value evaluation and self-control into behavioral choices. *Human Brain Mapping*, *40*(4), 1049–1061. https://doi.org/10.1002/hbm.24379

Zhao, L., Chen, C., Shao, L., Wang, Y., Xiao, X., Chen, C., … Xue, G. (2017). Orthographic and phonological representations in the fusiform cortex. *Cerebral Cortex*, *27*(11), 5197–5210. https://doi.org/10.1093/cercor/bhw300

SUPPORTING INFORMATION

Additional supporting information may be found online in the Supporting Information section at the end of this article.